VIP High-Pressure Zeolites

DOI: 10.1002/ange.201305230

Synthesis of a Novel Zeolite through a Pressure-Induced Reconstructive Phase Transition Process**

Jose L. Jordá, Fernando Rey, German Sastre, Susana Valencia, Miguel Palomino, Avelino Corma, Alfredo Segura, Daniel Errandonea, Raúl Lacomba, Francisco J. Manjón, Óscar Gomis, Annette K. Kleppe, Andrew P. Jephcoat, Mónica Amboage, and J. Alberto Rodríguez-Velamazán*

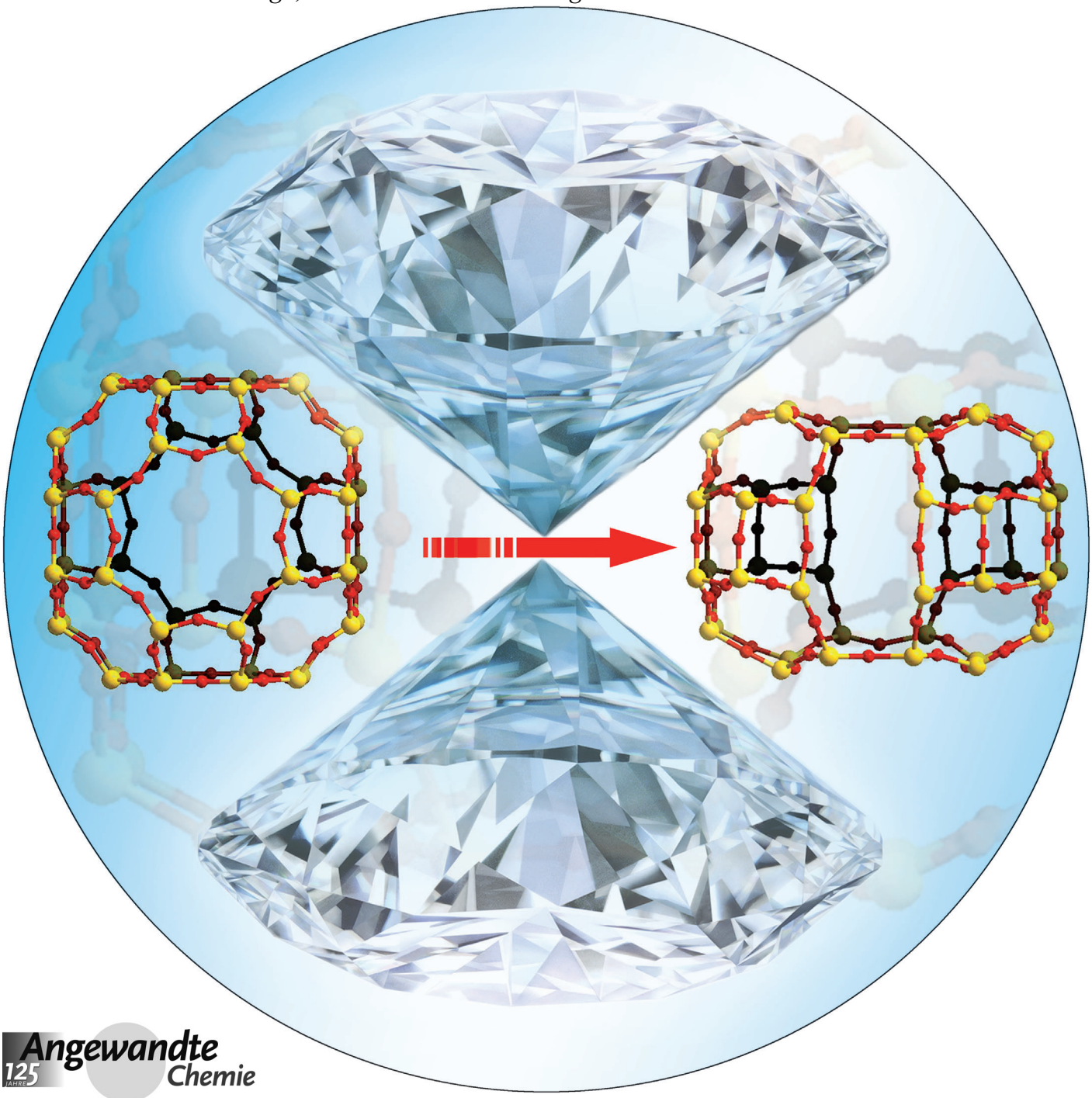

An understanding of pressure–temperature phase relations is needed for developing new methods for the synthesis of advanced solids.[1–3] In comparison to thermal treatments, the magnitude of changes in interatomic distances and coordination numbers of atoms is much larger under high pressure than under high temperature. Also, high temperature increases bond distances and atomic mobility, while high pressure generally has the opposite effect, opening unexplored routes for discovering new materials.[3] Importantly, many high-pressure phases retain their structures after returning to ambient pressure, which allows for their characterization and application. The advent of high-pressure devices able to reach pressures in the range of several hundred gigapascals (GPa), such as diamond anvil cells (DACs), has led to significant progress in the study of these new materials. Particularly successful has been the synthesis of highly dense materials such as new metals, semiconductors, super-hard abrasives, magnetic materials, gems, and specialized optical components, among others.[2–5]

One field of high-pressure research is the study of porous zeolitic materials. Zeolites are composed of silicon oxide and/or other elements, such as Al, B, or Ge, in tetrahedral coordination ($TO_{4/2}$). These tetrahedra are arranged into well-defined channels and cavities of molecular dimensions, and they confer to zeolites a broad range of applications in catalysis, separation, and adsorption processes.[5,6] Previous studies found that structural distortions of zeolites under high pressures were driven by tilting of the rigid $TO_{4/2}$ tetrahedra around bridging oxygens, with relatively low energy barriers, and by shortening of T–O distances, requiring higher energies.[7–9] Zeolites usually first undergo a phase transition in which the zeolite is converted into a low density amorphous (LDA) phase. This pressure induced amorphization (PIA) is reversible, and the original zeolite is recovered upon pressure release. In this order-to-disorder transition, the T-O-T angles change, whilst O-T-O angles and T-O distances remain unmodified.[10–14] Further compression leads to a high density amorphous (HDA) phase that does not revert back to the original zeolite. In this transition from LDA to HDA (called polyamorphism) some T–O bonds are broken, while new T–O linkages are formed.[10,11] Also, the presence of water associated to cations[15] and the nature of these cations has been found to be important in the response of zeolites to high pressures.[10,15a,16]

Previous high-pressure studies of zeolite A (LTA), with a Si/Al ratio close to one, have shown that its compressibility strongly depends on the ability of the pressure-transmitting medium (PTM) to penetrate into the zeolite pores.[17] Using non-penetrating fluids as PTM, Al-containing LTA follows the typical zeolite behavior with an LDA phase at relatively low pressures, while further pressure increase gives rise to the formation of an HDA phase.[10–12] Notably, a theoretical study predicted a reversible PIA in Al-rich LTA, with two amorphous phases, and also three PIA steps in pure-silica LTA, with only the first being reversible.[18]

Despite many high-pressure experiments performed on porous solids, it has not led to a new ordered zeolitic material. Therefore, it has been claimed that reconstructive phase transitions, with a change in topology, do not occur in tetrahedral SiO_2 polymorphs, feldspars, and zeolites.[8,11a]

The previous reports motivated us to do experiments on the high-pressure behavior of pure-silica LTA, named ITQ-29,[19] using non-penetrating PTMs. ITQ-29 combines the simplest zeolite structure (cubic symmetry with only one crystallographic silicon site and three independent oxygen positions) and very high stability.[19]

High pressure X-ray diffraction (XRD) experiments on ITQ-29 were performed, as described in the Supporting Information. Under pressure, ITQ-29 undergoes two transformations, and a new crystalline phase with no amorphization was formed (Figure 1). The first transformation, occurring at 1.2 GPa, is fully reversible and ITQ-29 is recovered upon pressure release. Most remarkable is the second transformation occurring at around 3.2 GPa (Supporting Information, Figure S1). This is an order-to-order reconstructive phase transition, non-reversible upon pressure release, pro-

[*] Dr. J. L. Jordá, Prof. F. Rey, Dr. G. Sastre, Dr. S. Valencia, M. Palomino, Prof. A. Corma
Instituto de Tecnología Química (UPV-CSIC), Universidad Politécnica de Valencia-Consejo Superior de Investigaciones Científicas
Av. de los Naranjos s/n 46022 Valencia (Spain)
E-mail: acorma@itq.upv.es

Prof. A. Segura, Prof. D. Errandonea, Dr. R. Lacomba
Instituto de Ciencia de Materiales de la Universidad de Valencia, MALTA Consolider Team, Universidad de Valencia
C. Dr. Moliner 50, 46100 Burjassot (Spain)

Prof. F. J. Manjón
Instituto de Diseño para la Fabricación y Producción Automatizada, MALTA Consolider Team, Universidad Politécnica de Valencia
Cno. de Vera, s/n, 46022 Valencia (Spain)

Dr. Ó. Gomis
Centro de Tecnologías Físicas: Acústica, Materiales y Astrofísica, MALTA Consolider Team, Universidad Politécnica de Valencia
Cno. de Vera, s/n, 46022 Valencia (Spain)

Dr. A. K. Kleppe, Prof. A. P. Jephcoat, Dr. M. Amboage
DIAMOND Light Source, Harwell Science and Innovation Campus
Didcot (UK)

Prof. A. P. Jephcoat
Department of Earth Sciences, University of Oxford
South Parks Road, Oxford, OX1 3AN (UK)

Dr. J. A. Rodríguez-Velamazán
Instituto de Ciencia de Materiales de Aragón (CSIC-Universidad de Zaragoza) at Institute Laue-Langevin, Grenoble (France)

[**] We thank the Diamond Light Source (beamline I15) and Institute Laue-Langevin (beamline D1B) for beamtime allocation, and the Spanish Government (projects MAT2010-21270-C04-01/04, MAT-2012-3856-C02-01, CTQ2010-17988/PPQ, Consolider MALTA CSD-2007-00045, Consolider Ingenio Multicat CSD-2009-00050 and program Severo Ochoa SEV-2012-0267), Generalitat Valenciana (Project Prometeo and GVA-acomp-2013-012) and "Vicerrectorado de Innovación y Desarrollo de la UPV" (PAID-05-2009, project UPV2010-0096) for financial support. G.S. thanks Centro de Cálculo (UPV) and Área de Informática Científica (SGAI-CSIC) for Computational facilities. We thank Dr. Vidal-Moya for ^{29}Si-MAS-NMR measurements and T. Portilla for technical support.

Supporting information for this article is available on the WWW under http://dx.doi.org/10.1002/anie.201305230.

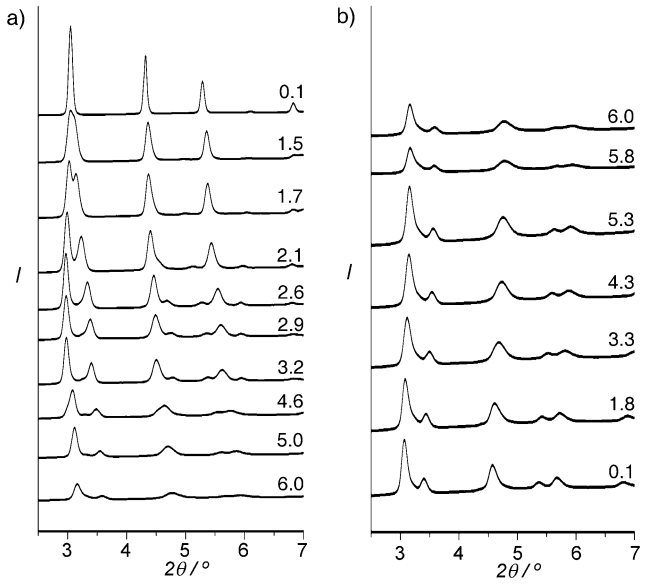

Figure 1. High-pressure synchrotron X-ray powder diffraction patterns ($\lambda = 0.619$ Å) of ITQ-29 using silicon oil as hydrostatic fluid in a DAC (right side number: pressure in GPa; top: starting material, bottom: final material). (a) Compression and (b) pressure release.

ducing a new material (named ITQ-50). Unfortunately, the low resolution of the in situ XRD data did not allow a complete structural analysis of ITQ-50 and only unit cell parameters were obtained from the X-ray diffraction patterns.

Neutron diffraction experiments (see Supporting Information) confirmed the previous results, but because of the very small amount of sample used, the resulting patterns were too noisy for a proper structural elucidation. However, it was possible to recover enough sample of ITQ-50 from this experiment to collect an XRD pattern in a laboratory X-ray diffractometer (Figure 2) to determine the framework structure.[20]

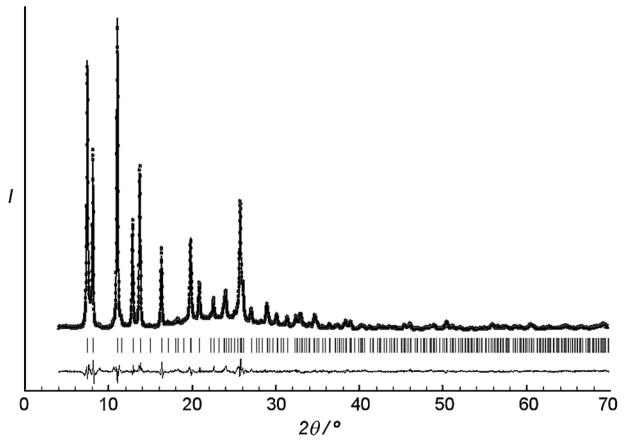

Figure 2. Rietveld refinement of the XRD pattern of ITQ-50 using $Cu_{K\alpha_1}$ radiation. Observed (circles) and calculated XRD patterns, as well as the difference profile (bottom) are shown. The short tick marks below the pattern give the positions of the Bragg reflections.

The parent ITQ-29 and the ITQ-50 materials are clearly different zeolites, as can be seen from their respective projections (Figure 3). While ITQ-29 contains only one Si site, ITQ-50 possesses four independent Si positions

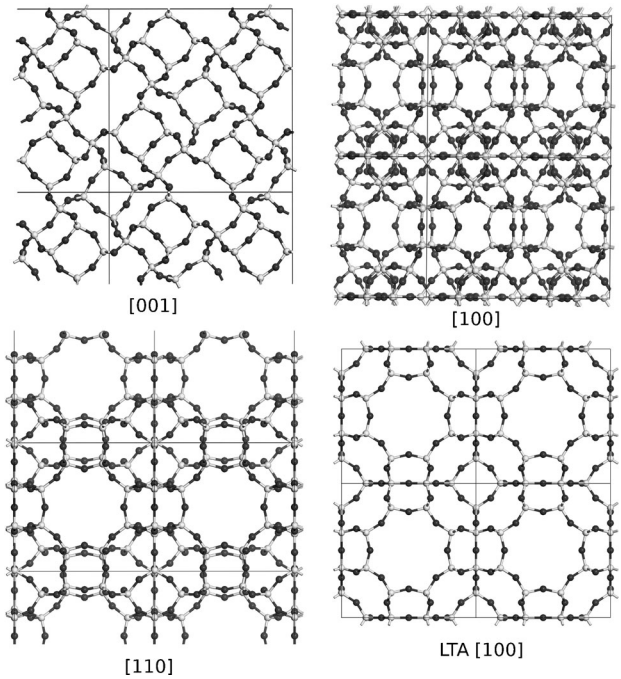

Figure 3. Projection of ITQ-50 along the main crystallographic directions ([001], [100], and [110]). Different 8R channels can be observed along [001] and [110]. Projection of ITQ-29 (LTA) along the [100] direction is also shown for comparison (Si gray, O black).

(Table S1). This difference is well supported also by ^{29}Si-MAS-NMR spectroscopy (Figure S2). The spectrum of ITQ-29 consists of a single resonance at $\delta = -112.8$ ppm, whereas the ITQ-50 material shows four sharp resonances at $\delta = -106.0$, -107.1, -109.8, and -111.7 ppm with relative intensities of 2:1:1:2, respectively.

Moreover, some substructures in both materials are clearly not coincident, although closely related. ITQ-29 can be described using three different composite building units (CBU), α-cage (*lta*), sodalite (*sod*), and double-four ring (*d4r*; Figure 4).[25] The α-cage has a ring content notation $[4^{12}6^{8}8^{6}]$. After the phase transition, the equivalent cage in ITQ-50, which has been named *ify*, can be described also as $[4^{12}6^{8}8^{6}]$; however, both cages are topologically different (Figure 4), owing to the change of the relative location of four 4R and two 8R. Also, only one half of the *d4r* cages present in ITQ-29 remains in ITQ-50; for the other half, the breakage of one of the edges converts the *d4r* units into *sti* units.[25] The sodalite cages remain intact during the transformation from ITQ-29 to ITQ-50, as previously described for Al-LTA.[11b]

Theoretical calculations were carried out to improve the understanding of the transformation of ITQ-29 into ITQ-50. The methodology and computational methods are described in detail in the Supporting Information.

The easiest tracking from the original α-cage to the final *ify* cavity involves three structural modifications (Figure 5). In

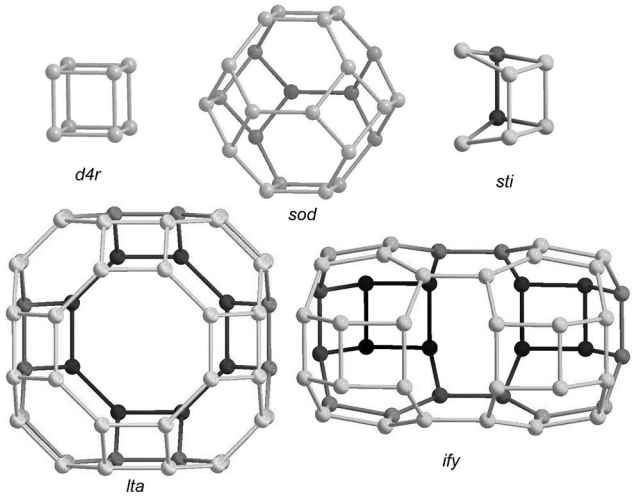

Figure 4. Composite building units of ITQ-29 (*d4r*, *sod*, and *lta*) and ITQ-50 (*d4r*, *sod*, *sti*, and *ify*). Oxygen atoms have been omitted for clarity.

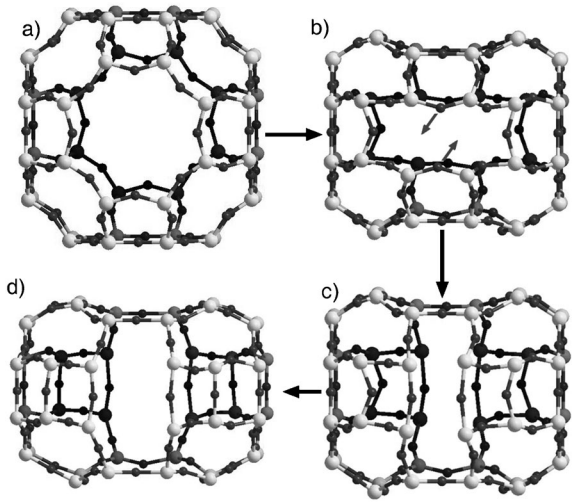

Figure 5. Suggested path from ITQ-29 to ITQ-50. a→b) Reversible deformation; b→c) Si–O bond breaking and formation through displacement of O atoms; c→d) structure relaxation.

the first step (a→b), a deformation is applied resulting in an α-cage compressed along one of the axes but retaining the original connectivity. In the second step (b→c), two Si–O bonds are broken and, after the displacement of those O atoms (shown in Figure 5b by the short arrows), two new Si–O bonds are formed between symmetrically equivalent Si atoms. In the third step (c→d), a framework relaxation is applied. If the same process is extended to the full ITQ-29 structure (steps A→D in Figure S4), a new unit cell is obtained, with a different connectivity corresponding to that of ITQ-50. Further energy minimization of this unit cell (steps D→G in Figure S4) provides the final ITQ-50 structure.

The cell parameters and volumes calculated from this theoretical mechanism are in good agreement with the experimental data (Figure S1), supporting the feasibility of this model. Also, the changes observed in the unit cell parameters with pressure are a good indication to ascertain the phase transitions. As shown in Figure S1, the a_s/c_s ratio of ITQ-29 remains constant from ambient pressure to 1.2 GPa, showing that the original cubic symmetry is retained. From 1.2 GPa to 3.2 GPa, the parameter c_s increases while a_s continuously decreases, reducing the a_s/c_s ratio. This is consistent with the tetragonal deformation in step a→b of Figure 5 and Figure S4; the retention of the framework connectivity is in good agreement with the reversibility observed. Further increase of the pressure above 3.2 GPa results in a reduction of c_s, with a constant a_s/c_s ratio. The non-reversibility of this second deformation can be attributed to the phase transition involving bond breaking and formation of new Si–O linkages (step b→c).

Finally, we have explored the ability of the new small pore zeolite ITQ-50 for the industrially important separation of propene and propane,[26] compared with that of ITQ-29. Figures S7 and S8 show the adsorption isotherms of propene and propane. The adsorption capacity of propene in ITQ-50 is lower than that in ITQ-29 (Table S5). This can be attributed to the higher framework density of ITQ-50 (17.3 versus 14.4 $SiO_2 \cdot nm^{-3}$) as well as to the decrease of the micropore volume upon deforming the spherical α-cage of ITQ-29 into the flattened *ify* of ITQ-50 (Figure 4 and 5). Notably, the drop of adsorption capacity of ITQ-50 is larger for propane than for propene, being an indication of stronger diffusion limitations for propane in ITQ-50 than in ITQ-29. This has been proven by conducting kinetic adsorption measurements (Figures S9,S10). Table S6 compares the calculated Fickian diffusion parameters (D_c/r_c^2) for these gases in ITQ-50 and ITQ-29, as well as the ratio of their diffusion coefficients (R_D), which gives a comprehensive indication of the ability of the solid for their separation. ITQ-50 gives a coefficient ratio of 158 that is more than four times larger than that of ITQ-29 ($R_D = 40$). The better propene/propane separation of ITQ-50 compared to ITQ-29 can be attributed to the presence of highly deformed 8R pores in ITQ-50 structure along the *c* axis, that preclude the diffusion of propane along this direction, resulting in a bidirectional-like channel system instead of the tridirectional pore topology of ITQ-29. Consequently, ITQ-50 could be an effective adsorbent for propene/propane kinetic separation.

In conclusion, we have undoubtedly shown that zeolites can be transformed into new zeolitic topologies through the effects of pressure, leading to the new zeolite ITQ-50 from the pure silica LTA topology (ITQ-29). The resulting ITQ-50 zeolite is an adequate material for conducting light olefin recovery from hydrocarbon mixtures, particularly for propene/propane separation.

Experimental Section

The ITQ-29 sample, which is the pure-silica form of zeolite A (LTA), was prepared as previously described,[19] and calcined at 1173 K for 8 h to remove all organic substances. Information regarding diffraction data collection, and crystallographic, computational and adsorption analysis is supplied as Supporting Information.

Received: June 18, 2013
Published online: August 1, 2013

Keywords: adsorption · high-pressure chemistry · phase transitions · X-ray diffraction · zeolites

[1] a) J. C. Joubert, J. Chenavas, *J. Solid State Chem.* **1979**, *27*, 29; b) P. F. McMillan, *Nat. Mater.* **2002**, *1*, 19.
[2] H. Huppertz, *Chem. Commun.* **2011**, *47*, 131.
[3] F. J. Manjón, D. Errandonea, *Phys. Status Solidi B* **2009**, *246*, 9.
[4] P. F. McMillan, *Nat. Mater.* **2005**, *4*, 715.
[5] M. E. Davis, *Nature* **2002**, *417*, 813.
[6] J. Jiang, J. Yu, A. Corma, *Angew. Chem.* **2010**, *122*, 3186; *Angew. Chem. Int. Ed.* **2010**, *49*, 3120.
[7] R. M. Hazen, L. W. Finger, *Phase Transitions* **1979**, *1*, 1.
[8] G. D. Gatta, *Microporous Mesoporous Mater.* **2010**, *128*, 78.
[9] G. D. Gatta, P. Comodi, P. F. Zanazzi, *Microporous Mesoporous Mater.* **2003**, *61*, 105.
[10] G. N. Greaves, F. Meneau, A. Sapelkin, L. M. Colyer, I. A. Gwynn, S. Wade, G. Sankar, *Nat. Mater.* **2003**, *2*, 622.
[11] a) G. N. Greaves, F. Meneau, F. Kargl, D. Ward, P. Holliman, F. Albergamo, *J. Phys. Condens. Matter* **2007**, *19*, 415102; b) J. E. Readman, P. M. Forster, K. W. Chapman, P. J. Chupas, J. B. Parise, J. A. Hriljac, *Chem. Commun.* **2009**, 3383.
[12] Y. Huang, E. A. Havenga, *Chem. Phys. Lett.* **2001**, *345*, 65.
[13] R. Arletti, O. Ferro, S. Quartieri, A. Sani, G. Tabacchi, G. Vezzalini, *Am. Mineral.* **2003**, *88*, 1416.
[14] J. Haines, C. Levelut, A. Isambert, P. Hébert, S. Kohara, D. A. Keen, T. Hammouda, D. Andrault, *J. Am. Chem. Soc.* **2009**, *131*, 12333.
[15] a) Y. Lee, T. Vogt, J. A. Hriljac, J. B. Parise, J. C. Hanson, S. J. Kim, *Nature* **2002**, *420*, 485; b) Y. Lee, C.-C. Kao, T. Vogt, *J. Phys. Chem. C* **2012**, *116*, 3286.
[16] a) M. D. Rutter, T. Uchida, R. A. Secco, Y. Huang, Y. Wang, *J. Phys. Chem. Solids* **2001**, *62*, 599; b) G. N. Greaves, F. Meneau, O. Majérus, D. G. Jones, J. Taylor, *Science* **2005**, *308*, 1299.
[17] R. M. Hazen, *Science* **1983**, *219*, 1065.
[18] I. Peral, J. Íñiguez, *Phys Rev. Lett.* **2006**, *97*, 225502.
[19] A. Corma, F. Rey, J. Rius, M. J. Sabater, S. Valencia, *Nature* **2004**, *431*, 287.
[20] The XRD pattern was indexed in a tetragonal unit cell ($a = 15.342$ Å, $c = 11.811$ Å) using the program TREOR,[21] consistent with the synchrotron and neutron diffraction data. Analysis of systematic extinctions suggested the possible space groups *P*4*bm* (No. 100), *P*-4*b*2 (No. 117), or *P*4/*mbm* (No. 127). The crystal structure was solved using the program FOCUS[22] with these three symmetries. Several possible frameworks were obtained and, after checking all of them, the first structure obtained using the highest symmetry (*P*4/*mbm*) was found to be correct. Oxygen atoms were placed between the tetrahedral Si atoms, and the structure was geometrically optimized using the program DLS-76.[23] Finally, the Rietveld refinement was performed using the program FULLPROF.[24] The residuals of the refinement were $R_{exp} = 0.053$, $R_{wp} = 0.114$, $R_F = 0.141$, and $R_B = 0.063$. Rietveld refinements using lower symmetries did not produce any improvement in the refinement. The agreement between the observed and the calculated patterns is shown in Figure 2. Measurement and refinement conditions, cell parameters, and atomic coordinates (Table S1) are given in the Supporting Information. Further details on the crystal structure investigations may be obtained from the Fachinformationszentrum Karlsruhe, 76344 Eggenstein-Leopoldshafen, Germany (fax: (+49) 7247-808-666; e-mail: crysdata@fiz-karlsruhe.de), by quoting the depository number CSD-426143.
[21] P. E. Werner, L. Eriksson, M. J. Westdahl, *Appl. Crystallogr.* **1985**, *18*, 367.
[22] R. W. Grosse-Kuntstleve, L. B. McCusker, C. Baerlocher, *J. Appl. Crystallogr.* **1999**, *32*, 536.
[23] Ch. Baerlocher, A. Hepp, DLS-76, Distance Least Squares Refinement Program, Institut für Kristallographie: ETH, Zurich, **1977**.
[24] J. Rodriguez-Carvajal, *CPD Newsletter* **2001**, *26*, 12.
[25] a) L. B. McCusker, F. Liebau, G. Engelhardt, *Pure Appl. Chem.* **2001**, *73*, 381; b) C. Baerlocher, L. B. McCusker, Database of Zeolite Structures: http://www.iza-structure.org/databases/, **2013**.
[26] a) S. U. Rege, R. T. Yang, *Chem. Eng. Sci.* **2002**, *57*, 1139; b) L. S. Cheng, S. T. Wilson, U. S. Patent 6296688, **2001**; c) R. T. Yang, E. S. Kikkinides, *AIChE J.* **1995**, *41*, 509; d) N. Hedin, G. J. DeMartin, K. G. Strohmaier, S. C. Reyes, *Microporous Mesoporous Mater.* **2007**, *98*, 182; e) R. B. Eldridge, *Ind. Eng. Chem. Res.* **1993**, *32*, 2208; f) C. A. Grande, J. Gascon, F. Kapteijn, A. E. Rodrigues, *Chem. Eng. J.* **2010**, *160*, 207.

